Duan *et al. Soft Sci.* **2025**, *5*, 4
DOI: 10.20517/ss.2024.46

Soft Science

Research Article

Open Access

A biocompatible integrated bladder electronics for wireless capacity monitoring assessment

Lin Duan, Ming-Liang Jin*

School of Automation, Qingdao University, Qingdao 266071, Shandong, China.

***Correspondence to:** Prof. Ming-Liang Jin, School of Automation, Qingdao University, Ningxia Road, Qingdao 266071, Shandong, China. E-mail: jinmingliang@qdu.edu.cn

How to cite this article: Duan, L.; Jin, M. L. A biocompatible integrated bladder electronics for wireless capacity monitoring assessment. *Soft Sci.* **2025**, *5*, 4. https://dx.doi.org/10.20517/ss.2024.46

Received: 20 Sep 2024 **First Decision:** 24 Oct 2024 **Revised:** 13 Nov 2024 **Accepted:** 29 Nov 2024 **Published:** 17 Jan 2025

Academic Editors: Seung Hwan Ko, Carlo Massaroni **Copy Editor:** Ting-Ting Hu **Production Editor:** Ting-Ting Hu

Abstract

The real-time assessment and personalized monitoring of human bladder status is important for individuals with involuntary voiding, overactive bladder and bladder disorders such as urinary incontinence. To address the shortcomings of traditional urodynamic methods where the equipment is bulky, complex, invasive, expensive and unable to continuously monitor bladder status, and to meet the needs of healthcare professionals and family members to know the patient's bladder capacity, this paper designs the biocompatible integrated bladder electronics for wireless capacity monitoring assessment. The device employs chitosan, which exhibits favorable biocompatibility, to fabricate patch electrodes, and optimizes their performance through the plasticizing effect of glycerol, with a polarization resistance of 4.8983 kΩ, a maximum tensile force of up to 107.5 kPa, and remains chemically stable for long-term wear. The principle of bioelectrical impedance analysis is employed to integrate a hardware system comprising multiple modules, including a microcontroller, information processing, communication, display and power supply. After the integrated system design is completed with electrodes connected and encapsulated, data on bladder electrical impedance changes is gathered and transmitted wirelessly to the user interface for non-invasive real-time monitoring and intelligent assessment of bladder capacity. The experimental results demonstrate a high correlation between human bladder electrical impedance and bladder volume, with a systematic measurement correlation coefficient reaching 96.7%. The research equipment is portable, simple to operate, and radiation-free to the human body. It has significant potential for real-time monitoring and intelligent alarm of bladder capacity.

Keywords: Bladder disease, biocompatible electrodes, bioelectrical impedance analysis, integrated wearable electronics, wireless capacity monitoring

INTRODUCTION

The bladder is a functional organ responsible for storing urine and releasing it at the appropriate time[1-3]. The process of normal urination is a conscious, controlled neurological reflex activity that is accomplished through a complex series of neural reflexes and feedback mechanisms[4,5]. Bladder stimulus impulses are transmitted through sensory fibers of the parasympathetic nerves to the spinal reflex arc, which subsequently passes through the thin bundles in the spinal cord to the higher urinary centers in the brain, thus producing the urge to urinate. Upon the onset of the urge to urinate, motor impulses are transmitted to the bladder via the neurological reflex arcs, pelvic nerves, and parasympathetic efferent fibers, resulting in the excretion of urine[5-7]. A number of factors, including neurological disorders, incomplete brain development, urinary tract infections, structural abnormalities, and others, can result in urinary dysfunction. Overactive bladder (OAB) is a common bladder dysfunction, with urinary frequency, urgency, and incontinence as the main symptoms. This condition has a significant impact on the quality of life of many individuals, yet there is still a significant diagnostic and therapeutic gap in many countries. The International Continence Society survey indicates that approximately 25 million middle-aged adults experience transient or chronic urinary incontinence, defined as involuntary voiding and uncontrolled urine leakage. Of these, 9 to 13 million patients experience severe symptoms[8]. In older adults and children aged 2 years and younger, incontinence occurs more commonly. In clinical settings, OAB, neurogenic bladder (NGB), and urgency urinary incontinence (UUI)[9-12] are frequently attributed to neurological disorders or spinal cord injuries (SCI) that disrupt the normal functioning of the lower urinary tract. Consequently, it is imperative for medical professionals and family members to be aware of and analyze the patient's bladder capacity in real time [Figure 1A]. Overall, bladder dysfunction continues to impose a significant morbidity burden in many countries. It is therefore important to strengthen efforts to prevent and diagnose bladder disorders at an early stage, with the aim of improving the quality of life and health of those affected.

In clinical practice, real-time monitoring of bladder function is critical for managing various urinary disorders, enhancing patient comfort, and preventing complications associated with urinary retention or incontinence. The accurate assessment of bladder volume and capacity is essential in diagnosing dysfunctions such as OAB, NGB, and urinary retention. However, current bladder monitoring methods face substantial limitations. Currently, the principal bladder capacity and volume monitoring devices employed in clinical practice are ultrasonography (ultrasound, US)[13,14], urinary flow rate testing (urinary catheters, UC, uroflowmetry)[15,16], bladder pressure-volume testing[17], magnetic resonance imaging (MRI)[18,19] and computer tomography (CT)[20]. These methods, while useful, are generally limited in their application due to either invasiveness, high cost, or limited accessibility for real-time monitoring. For instance, US requires the use of specialized equipment that is both large in size and demands a high level of expertise from the user, and although individual wearable bladder monitoring devices exist, they are expensive to purchase. Uroflowmetry typically necessitates that the patient urinates in a natural state and can be employed as a screening instrument by documenting the rate and duration of urine flow to ascertain bladder capacity. Bladder pressure-volume testing (bladder pressure-volume relationship) necessitates the insertion of a catheter, which is an invasive procedure with an increased risk of infection. MRI necessitates the placement of the patient's body within a robust magnetic field, is costly to equip, and is subject to volume limitations. It is therefore unsuitable for use in overweight and anxious patients. Computed tomography employs X-ray fluoroscopy and an inverse projection algorithm to obtain a tomographic image of the bladder. Substances such as metal implants may cause artifacts, affecting the quality of the image, and there is a degree of radiation risk. In conclusion, while existing methods offer significant advantages for bladder monitoring, they are generally constrained to specific environments and are not well-suited for real-time or remote monitoring applications due to issues such as high costs and invasiveness. Therefore, developing a bladder

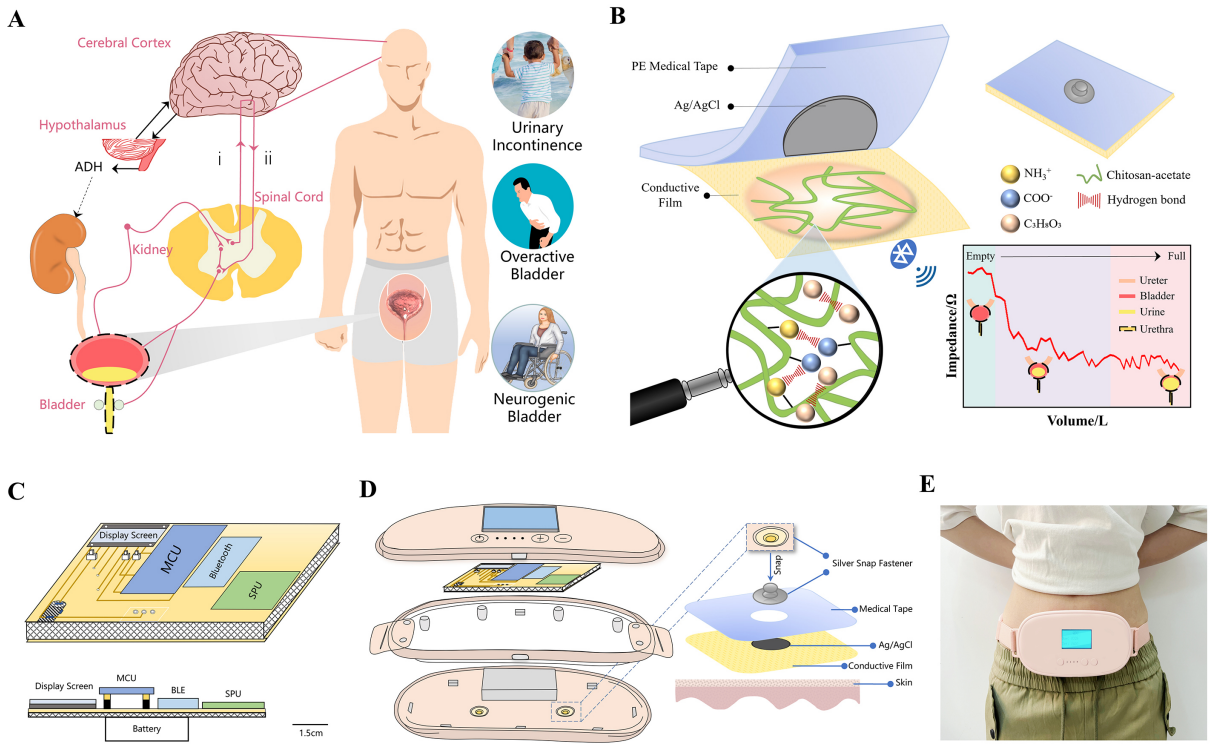

Figure 1. Architecture of a biocompatible integrated bladder electronics device for wireless real-time monitoring. (A) The mechanism of human urination; (B) Signal acquisition using chitosan-acetic acid electrodes; (C) A cutaway view (top) and longitudinal section (bottom) of the system hardware circuit board(8 cm × 8 cm); (D) The packaging of the electronics and the connection to the patch electrodes; (E) Photograph of adult females wearing the fully integrated electronics, and the device's overall housing dimensions are specified as 16 cm × 8 cm. ADH: Antidiuretic hormone; MCU: microcontroller unit; SPU: signal processing unit; BLE: bluetooth.

monitoring technology that is cost-effective, lightweight, portable, non-invasive, non-radioactive, and capable of real-time monitoring remains a significant challenge.

In this paper, we will present a novel approach to the development of wireless electronics for real-time monitoring and intelligent assessment of bladder capacity. The electronics integrate biocompatible material synthesis, bioelectrical impedance analysis (BIA), and multi-module system integration technologies to continuously monitor the status information of the bladder in real time, offering a solution for individuals with varying needs, including people with no sense of voluntary urination and patients suffering from urinary incontinence or OAB disorder. The device comprises two components: one is chitosan-acetate patch electrodes. The flexible substrate material, which comes into direct contact with the human skin, employs chitosan, which is biocompatible and exhibits strong adsorption properties. This reduces the risk of inflammatory and allergic reactions caused by bacterial and fungal infections, while also ensuring that the user experiences optimal comfort over an extended period of time[21-23]. Furthermore, glycerin, a green solvent, is selected as the base plasticizer. This is achieved through the intermolecular ester bonding, hydrogen bonding and gap-filling mechanism, which collectively enhance the softness, ductility and toughness of the conductive film[24-26] [Figure 1B]. Additionally, the electrode's overall structure is designed as a sandwich structure, effectively increasing the contact area between the electrode and the skin. The other component is a hardware system that is integrated with a number of modules, including a display, a microcontroller, an information processing unit, a communication system and a power supply[27] [Figure 1C]. After the printed circuit board (PCB) design is completed, the board is encapsulated and the biocompatible electrodes are connected to the hardware system. This integration of the electronic device for

bladder monitoring is achieved when the device is used by the user [Figure 1D]. The system employs BIA to monitor and automatically analyze bladder capacity non-invasively and in real time by current conduction, after applying a weak alternating current (usually 50 kHz) to the surface area of the bladder[28,29]. This is achieved by using a sensor to measure the voltage change as the current passes through the human bladder, which allows for the collection of information on the change in electrical impedance of the bladder. This information is then communicated wirelessly with the user interface (UI) (mobile phone app). Figure 1E depicts a live view of the user wearing the smart device on the abdomen. Supplementary Table 1 shows a comparison of conventional and development equipment in terms of dimensions.

This fully integrated biocompatible electronics for real-time monitoring and intelligent assessment of human bladder impedance employs a non-invasive methodology to provide real-time, continuous bladder filling information. It is portable and user-friendly, facilitating patient understanding of their needs. By anticipating the time of urination, the electronics enable patients or their family members to prepare in advance and reduce the likelihood of embarrassing instances of involuntary urination. In instances where medical science has yet to develop a cure for urination disorders, the human bladder impedance measurement smart device, developed using biocompatible electrode synthesis, BIA and multi-module system integration technology, enhances the patient's control over the time of bladder emptying and reduces the patient's psychological pressure, thereby improving the quality of life.

EXPERIMENTAL

Materials and instruments

Chitosan ($C_{6n}H_{11n}NO_{4n}$, MW = 100,000), acetic acid solution (CH_3COOH, MW = 60.05), sodium hydroxide standard solution (NaOH, 0.1 mol/L), potassium hydroxide (KOH, MW = 60.05, 95%), magnesium chloride ($MgCl_2$, 99%, MW = 95.21), glucan ($C_{6n}H_{10n}O_{5n}$, MW = 1,500) and deionized water were supplied by Macklin Biochemical Co., Ltd., Shanghai, China. Ethanol (C_2H_5OH, 95%) and potassium chloride (KCl, MW = 74.55) were purchased from Sinopharm Chemical Reagent Co., Ltd., Shanghai, China. Urea (H_2NCONH_2, 99.0%) was obtained from Tianjin Third Chemical Plant Co., Ltd., Tianjin, China. Ascorbic acid ($C_6H_8O_6$, MW = 176.13) was obtained from Yatai United Chemical Co., Ltd., Wuxi, China. The KEWLAB analytical balance was purchased from Qiulai Technology Co., Ltd., Hangzhou, China. Benchtop magnetic stirrer (model SC-MS-II) and benchtop homogenizer (model KW-4BC) were purchased from Cedex Electronics Co., Ltd., Beijing, China. The electric heating blast drying oven (model DHG-9145A) was obtained from Yiheng Scientific Instrument Co., Ltd., Shanghai, China. The Series 7 force gauge was purchased from MARK-10 Corporation, USA. The Autolab electrochemical workstation (model Nova2) was purchased from Metrohm Autolab B.V. through Maiqiang Technology Co., Ltd., Shanghai, China.

Design and performance study of patch electrodes

Patch electrode sensing is a non-invasive electrophysiological measurement for the assessment of bladder capacity. Its design is based on the conductive and capacitive response of biological tissues to electrical currents[1,30]. The system employs a two-electrode configuration, comprising a working electrode (WE) and a counter electrode (CE). The CE injects low-frequency alternating current (LFAC) into the human bladder, while the WE serves as a receiver electrode, collecting information about the bladder variable. This variable is generated due to the conductivity and capacitance of the bladder tissues in response to the current. Given the necessity for direct contact between the patch electrode and the human skin and the potential for long-term monitoring of bladder impedance, it is essential that the electrode exhibits good biocompatibility, anti-stretching properties, selectivity, and durability. This is to prevent the occurrence of undesirable reactions, such as allergies and inflammation, that may arise due to prolonged contact[31-33]. In light of these considerations, chitosan was selected as the primary material for the flexible substrate of the electrode. Chitosan is a natural polymer material with a strong affinity for human cells. It exhibits excellent properties,

including antibacterial, antiviral, fully biocompatible and biodegradable characteristics[22,34,35]. The green solvent glycerol was selected as the plasticizer for the flexible substrate, which contains a multitude of hydroxyl groups in its molecular structure and is capable of reacting with the numerous carboxyl groups present in the chitosan-acetic acid mixed solution. The glycerol generates ester bonds and forms strong hydrogen bonding interactions with the polymer molecules in the solution, thus improving the softness, ductility and toughness of the base film. Furthermore, the moisturizing properties of the chitosan substrate are exploited to prolong its service life[36]. Chitosan films offer several advantages over gels traditionally based on polyacrylic acid and polyvinyl alcohol. These include a lower cost, a lower risk of allergic inflammation such as itching and redness due to chitosan's good biocompatibility, and a higher breathability[37].

The fabrication process of the biocompatible electrode patch film for bladder monitoring is illustrated in Figure 2A and the Supplementary Materials. The structural properties of chitosan, which comprises free amino groups in its molecules, are exploited to convert its glucose amino groups to R-NH_3^+ in dilute acid, thereby forming a polycationic gel solution [Supplementary Figure 1][38,39]. These positively charged chitosan particles are susceptible to electrostatic adsorption on negatively charged biological skin, while the amino groups inhibit bacteria by binding to the negative electrons of human skin [Figure 2B]. The chitosan gel was electrochemically modified using glycerol, and the stress-strain curve (σ-ε curve) and open-circuit potential-electrochemical impedance spectroscopy (OCP-EIS) were employed to further characterize the electrode flexible substrate following modification with different volumes of glycerol [Figure 2C and D]. As the concentration of glycerol increased, the peak stress in the σ-ε curve exhibited an upward trend, while the resistance in the Nyquist plot exhibited a downward shape. This indicates that the tensile strength and conductivity of the film were increasing. It is noteworthy that, in the σ-ε curve, a decrease in flexibility was observed when the volume of glycerol exceeded 6%. This can be attributed to glycerol's plasticizing effect, whereby glycerol esters exhibit high resistance to fracture and can form a protective film to enhance the tensile strength and flexibility of the material. When the glycerol concentration exceeds the optimal level, it exerts a plasticizing effect, leading to a reduction in the toughness of the film. It is also important to control the amount of glycerol added in the experiment, as too much or too little will affect the performance of the membrane. Given that the biocompatible chitosan membrane in this paper is a flexible substrate that needs to be worn for a long period of time and come into direct contact with the human body to conduct signals, we chose to increase the volume of glycerol to 8%, in order to provide maximum tensile strength and conductive ability for bladder status monitoring and analysis. To evaluate the compatibility of the chitosan-acetic acid conductive film with human skin, we measured the surface energy of the film using a surface contact angle goniometer. The contact angle of water on the film was found to be 87.1°, while that of diiodomethane was 42.7° [Supplementary Figure 2A]. Using the Owens-Wendt theory, we calculated the surface energy of the chitosan film to be 39.95 mJ/m^2. This surface energy value is close to the range of surface energy for human skin (35-45 mJ/m^2), indicating that the material possesses good biocompatibility, making it suitable for applications in skin-contacting wearable devices[40,41]. Furthermore, we conducted skin irritation tests to assess the changes in skin condition over time after wearing the conductive film[42] [Supplementary Figure 2B]. No significant redness or itching was observed on the skin following the removal of the patch, providing clear evidence of the material's excellent biocompatibility. The patches were characterized for tensile strength, mechanical bending and adhesion [Supplementary Figure 3A-C].

Figure 2E presents a voltammetry characteristic curve of the chitosan-acetate conductive film at different rates (5-30 mV/s) within the voltage range of -1.5-1.5 V. The results demonstrate that the peak value of the voltammetry characteristic curve increases with the rate, indicating that the charge transfer within the film is more active at higher rates [Supplementary Figure 4A]. This implies that the film has a superior fast

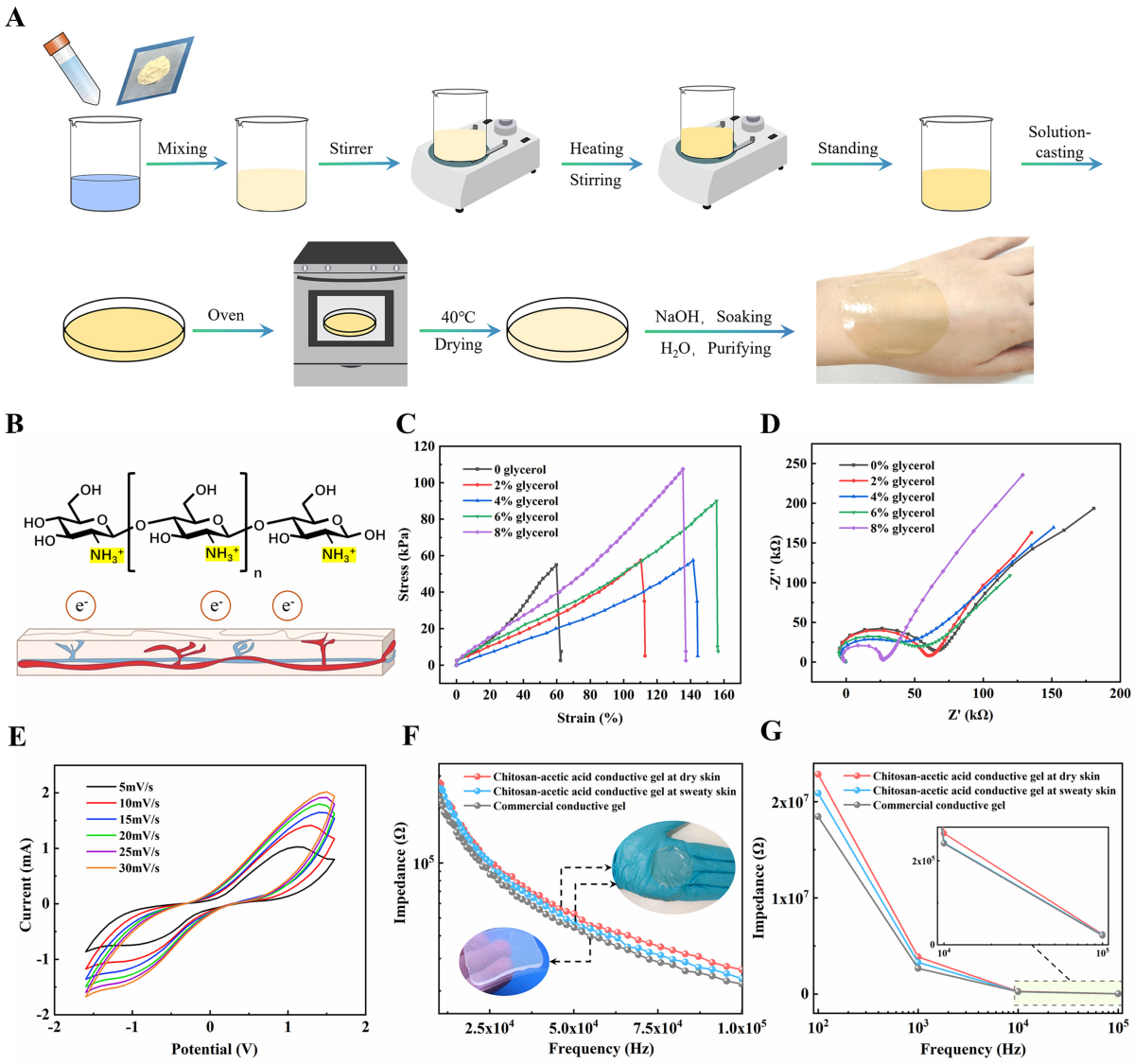

Figure 2. The preparation process and performance of biocompatible electrode patch. (A) The preparation process of the chitosan-acetate biocompatible conductive film; (B) The adhesion mechanism of the chitosan-acetic acid biocompatible conductive film; (C and D) Stress-strain curve alterations and impedance modifications following the formation of films through the addition of glycerol at varying volume ratios; (E) Volt-Ampere characteristic response of chitosan-acetate (8%) flexible films at varying scan rates; (F and G) The impedance-frequency curve response of a commercial conductive gel and chitosan-acetic acid conductive gel under both dry and sweaty human skin conditions.

response capability. Furthermore, the more gradual change in peak value indicates that the film has superior stability and consistency in electrochemical performance. Figure 2F illustrates the impedance-frequency curve response of a commercial conductive gel and chitosan-acetate conductive gel film, in both human dry skin and sweaty skin conditions. The frequency-impedance response of the commercial conductive gel is examined solely on dry skin, as it is a gel electrolyte-loaded electrode and therefore perspiration does not affect the impedance[37,43]. This group served as a control group, and the Nova2 electrochemical workstation was selected as the experimental measurement equipment for all experimental groups. Compared to impedance on dry skin, perspiration on the skin increased the effective conducting ions and decreased the current loading capacity, resulting in chitosan-acetate gel exhibiting less impedance overall on sweaty skin[44]. Chitosan-acetate gel exhibited slightly larger impedance values than commercial gel, with the

difference in impedance between the two gradually converging to 0 with increasing frequency, further validating the usability of the chitosan-acetate gel. As illustrated in Figure 2G, the impedance difference between the commercial gel and the chitosan-acetate gel is considerable at low frequencies of 10 and 100 Hz. The impedance of the chitosan-acetate gel and commercial conductive gel under dry skin is 2.0886e7 and 1.8449e7 Ω, respectively, with an error rate of 13.21%. At 10^3, 10^4, and 10^5 Hz, the error rate decreased gradually to 0.561%. At higher frequencies, the effect of frequency on the impedance is weakened. This is due to the fact that as the frequency increases, the signal tends to be distributed on the surface of the conductor, resulting in a decrease in current density and inductance. At a certain frequency, the decrease in inductance can be ignored and remains unchanged, resulting in a stabilized change of impedance[45,46]. In this study, 50-60 kHz was selected as the measurement frequency for the human bladder impedance. At this frequency range, the chitosan-acetate gel exhibited lower impedance and superior conductivity. Furthermore, the chitosan-acetate electrode patch demonstrated enhanced conductivity across a range of frequencies in comparison to the commercial conductive gel electrode patch [Supplementary Figure 4B].

RESULTS AND DISCUSSION

Analysis of measurement and design principles for wireless electronics

The state change of the human bladder tissue exhibits nonlinear behavior, which is dependent on the dielectric constant and frequency. BIA is a technique that measures the electrical properties of biological tissues to assess their physiological status. In the context of bladder monitoring, BIA works by applying a small alternating current through the bladder tissue and measuring the resultant impedance. We employed multi-frequency BIA as a technique to measure tissue resistance across various biological structures. Different tissues, such as fat, muscle, and skin, exhibit unique conductive properties; thus, using multi-frequency signals enables us to quantify each tissue's contribution to total impedance. Low-frequency currents primarily traverse the extracellular fluid, allowing us to measure fat thickness and other characteristics, while high-frequency currents penetrate cell membranes and access intracellular regions. By analyzing data across multiple frequencies, we can distinguish impedance characteristics among fat, subcutaneous tissue, and surrounding bladder tissues, allowing for an accurate calculation of bladder impedance. Changes in impedance are sensitive to variations in bladder volume, as these affect the distribution and properties of intracellular and extracellular fluids[47]. This phenomenon is characterized by non-uniform phenomena such as charge migration during the change[48].

As illustrated in Figure 3A, the inner membrane of the bladder is observed to be full of folds when the bladder is initially empty. With the accumulation of urine, the increased bladder volume gradually unfolds the bladder membrane, resulting in a smoother inner membrane surface. This unfolding process affects the dielectric properties of the bladder tissue, which in turn influences the impedance values measured by BIA. Specifically, as the bladder fills, the capacitance of the intracellular membrane decreases, reflecting changes in tissue structure. Simultaneously, the intracellular fluid resistance of the bladder cells increases due to urine accumulation, while the extracellular fluid resistance of the bladder cells remains relatively stable[49,50].

In light of the aforementioned considerations, the Cole-Cole model was selected to elucidate the intricate electrical dynamics observed in the bladder[51]. This model has a multitude of applications, including the investigation of conductivity, dielectric constant, and resonant frequency in dielectric materials. By applying the Cole-Cole model to bladder tissue, it is possible to create an equivalent electrical model that accurately reflects the impedance characteristics of a single bladder cell under different volume conditions. In this instance, the equivalent model of bioelectrical impedance of a single cell in bladder tissue is depicted in Figure 3B.

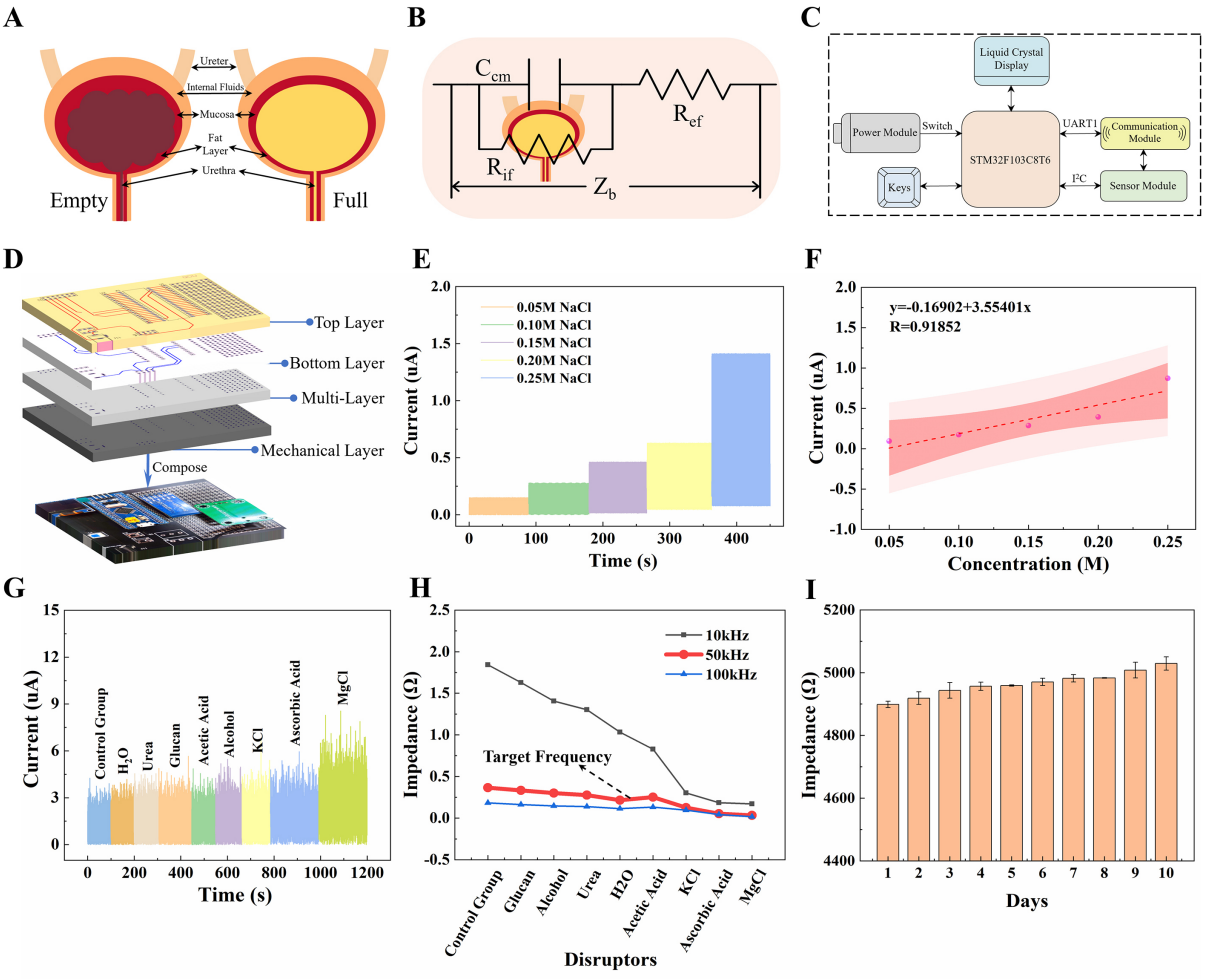

Figure 3. Integrated design principle and performance characterization of the wireless monitoring electronics. (A) Structural characteristics of the bladder; (B) Bioelectrical impedance equivalent model of individual cells of the bladder tissue; (C) The hardware block diagram of the microcontroller system; (D) Schematic diagram of the main control board of electronics; (E) The amperage response of varying concentrations of NaCl solution (0.05-0.25 M) was applied to the electrode patch; (F) Linearity and regression model between response current height and solution concentration; (G) The immunity and selectivity of the system to different interfering molecules; (H) The system demonstrates immunity to interfering molecules at varying frequencies; (I) The impedance variation and stability of the bladder sensor over a period of ten days.

The mode and phase of the bladder impedance Z_b are calculated as follows, and the calculation process is presented in the Supplementary Materials:

$$|Z_b| = \sqrt{\frac{\left[R_{ef}\left(1+R_{if}^{\ 2}\omega^2 C_{cm}^{\ 2}\right)+R_{if}\right]^2 + R_{if}^{\ 4}\omega^2 C_{cm}^{\ 2}}{\left(1+R_{if}^{\ 2}\omega^2 C_{cm}^{\ 2}\right)^2}} \tag{1}$$

$$\theta_{Z_b} = -\tan^{-1}\left[\frac{\frac{R_{if}^{\ 2}\omega C_{cm}}{1+R_{if}^{\ 2}\omega^2 C_{cm}^{\ 2}}}{\frac{R_{ef}\left(1+R_{if}^{\ 2}\omega^2 C_{cm}^{\ 2}\right)+R_{if}}{1+R_{if}^{\ 2}\omega^2 C_{cm}^{\ 2}}}\right] \tag{2}$$

In conclusion, the observed trend of parameter alterations and the substitution of the expression for bladder impedance, Z_b, leads to the conclusion that human bladder impedance, Z_b, decreases as urine storage volume increases. Consequently, researchers can further ascertain the state of the human bladder by investigating the nonlinear inverse relationship between the change in urine storage volume and the change in bladder impedance.

Integration and characterization of a wireless electronics

A fully integrated wireless bladder status monitoring electronic device was developed based on the assembly of a biocompatible electrode patch and reusable PCB. The PCB contains a microcontroller unit (MCU), in which STM32F103C8T6 serves as the terminal master controller with a high-performance and low-power 32-bit RISC processor ARM Cortex-M4, a diverse range of peripheral interfaces, including a timer, an analog-to-digital converter (ADC), inter-integrated circuit (I^2C), and communication interfaces such as a universal asynchronous receiver/transmitter (UART) and a serial peripheral interface (SPI)[52,53]. This internal special composition facilitates communication with other modules on the board or external smartphones. The hardware block diagram of the system, which employs the STM32F103C8T6 as the principal controller, is depicted in Figure 3C. This diagram includes the UART1 serial port circuit, keypad, and liquid crystal display (LCD). This design is to eliminate the host computer and integrate the programmable low-power Bluetooth (BLE) module for remote data transmission and monitoring between the devices. The module is integrated with a microcontroller for signal processing and wireless communication, Supplementary Figure 5A and B illustrates the BLE module schematic and pin diagram, and microcontroller system for UART serial communication, the communication protocol that is the UART communication protocol. The microcontroller's receive (RX) and transmit (TX) ports are connected to the corresponding ports on the JDY-31 module, enabling the transmission of data and receipt of commands. Furthermore, the device incorporates a signal processing unit (SPU) and three buttons, which serve as the overall on/off key of the system and the key for setting alarm thresholds[54]. Additionally, it features an LCD for real-time display of monitoring data and a rechargeable 5 V lithium battery with a capacity of 2,400 mAh for power supply. This is followed by the fabrication of the board [Figure 3D].

After designing the schematic based on the overall system architecture and hardware requirements, it was imported into the PCB design software, Altium Designer. The circuit board was partitioned and layered according to electrical performance requirements. The mechanical layer was configured to set the dimensions and mechanical details of the main control board, while the signal layer was used for component placement, routing, and soldering. The component layer was designated for resistor soldering and silkscreen printing. Signal, ground, and power lines were routed in the inner layers to ensure compliance with impedance control standards. Component positions were adjusted accordingly to finalize the PCB layout, and the board was subsequently prepared for fabrication[55,56]. Further details can be found in the Supplementary Materials.

The efficacy of this wireless monitoring system was assessed by spraying varying concentrations of NaCl solution (0.05-0.25 M) onto the electrode patches of the fully integrated electronic system [Figure 3E], which was selected due to the substantial presence of chloride and sodium ions in human sweat. The system exhibited a linear relationship between the height of the response current and the concentration of the solution, with a regression model as shown in Figure 3F, with a correlation coefficient of 0.9185. Furthermore, the system demonstrated the same linear relationship at different frequencies [Supplementary Figure 6A]. Figure 3G illustrates the resultant plot of the system monitoring in the presence of interfering molecules in sweat. A series of interfering molecules, including H_2O, urea, dextran, acetic acid, ethanol, potassium chloride, ascorbic acid, and magnesium chloride, were sprayed onto the electrode surface. In contrast, the control group mimicked dry human skin without spraying the solutions. The responses were

then tested sequentially. The presence of these interfering molecules had no significant effect on the current response, confirming the good selectivity of the system. In particular, the immunity of the system was measured at 10, 50 and 100 kHz [Figure 3H and Supplementary Figure 6B], where the impedance change was large at 10 kHz. This indicates that the interfering molecules will be somewhat disruptive to the system at low frequencies. In contrast, the impedance change was weak at the experimental frequency chosen in this paper, 50 kHz. This again confirms the suitability of the system. Long-term stability is a critical factor for sensor performance, particularly in applications requiring consistent measurements over extended periods. Stability can be influenced by material degradation, environmental fluctuations, and repetitive loading[57]. To minimize impedance drift over time, this study implemented measures such as optimizing electrode material properties and applying protective encapsulation to limit external influences. The stability of the device materials during long-term usage is further discussed in Supplementary Table 2. Additionally, the impedance changes of the bladder sensor were measured over a 10-day period, as shown in Figure 3I, to assess its long-term stability. The sensor was applied to the human skin and the impedance was measured every 24 h. The results demonstrated that the relative standard deviation (RSD) of the sensor was 0.791%, which confirmed the operational stability of the system.

Validation and evaluation of a wireless bladder electronic device

During the process of bladder emptying to filling, urine storage continues to rise and impedance values tend to decrease, as shown in Figure 4A. The utilization of wearable technology for the analysis of human bladder impedance represents a low-risk, low-cost and easy-to-use approach to the remote monitoring of patients or family members, when compared to invasive and US-based analyses. In order to validate the value of the designed electronic device for measuring bladder status, six participants of varying ages (three males and three females) were monitored for bladder status. Prior to the commencement of the experiment, the skin of the subject must be cleaned and sterilized. Thereafter, two measurement electrodes are to be adhered to the lower abdomen of the subject in a symmetrical manner, at a point 10 cm below the navel and 5 cm from the midline of the navel[58,59]. The electrodes are mounted in the position illustrated in Figure 4B. The designed electronics and the commercial equipment were connected to the electrodes, and the appropriate measurement parameters were set: start frequency 50 kHz, termination frequency 60 kHz.

Following the emptying of the bladder by the tester, the designed electronics and commercial equipment were activated for a 30 min measurement of the bladder impedance. After 30 min, the tester consumed 500 mL of drinking water in one sitting, maintaining the designated sitting posture. Initially, the measurement was conducted using commercial equipment. The current frequency delivered to the electrodes was 50 kHz, with a frequency scanning interval of 1 min, enabling the bladder electrical impedance to be measured at regular intervals[60]. Subsequently, the measurement was conducted using a designed electronics. The bladder electrical impedance per minute was recorded by observing the data displayed on the LCD screen on the system board or the mobile phone application [Figure 4C]. The measurement process continued until the tester indicated that they wished to urinate, at which time the tester's bladder was in a full state. Following the conclusion of each experimental series, the data obtained from the two groups of devices were subjected to comparison and analysis. The resulting measurement outcomes are presented in Figure 4D-I.

The test results indicate that the magnitude and rate of change in bladder impedance may exhibit inter-individual variation across participants over time. This is consistent with the increase in bladder volume as the bladder fills with urine. The converted impedance data showed a decreasing trend in bladder impedance as urine accumulated, indicating an increasing trend in bladder volume. Particularly, bladder impedance decreased rapidly approximately 10 min after participants drank water. Upon reaching a predetermined threshold, the mobile device would activate a continuous vibration alarm to prompt the user to urinate promptly.

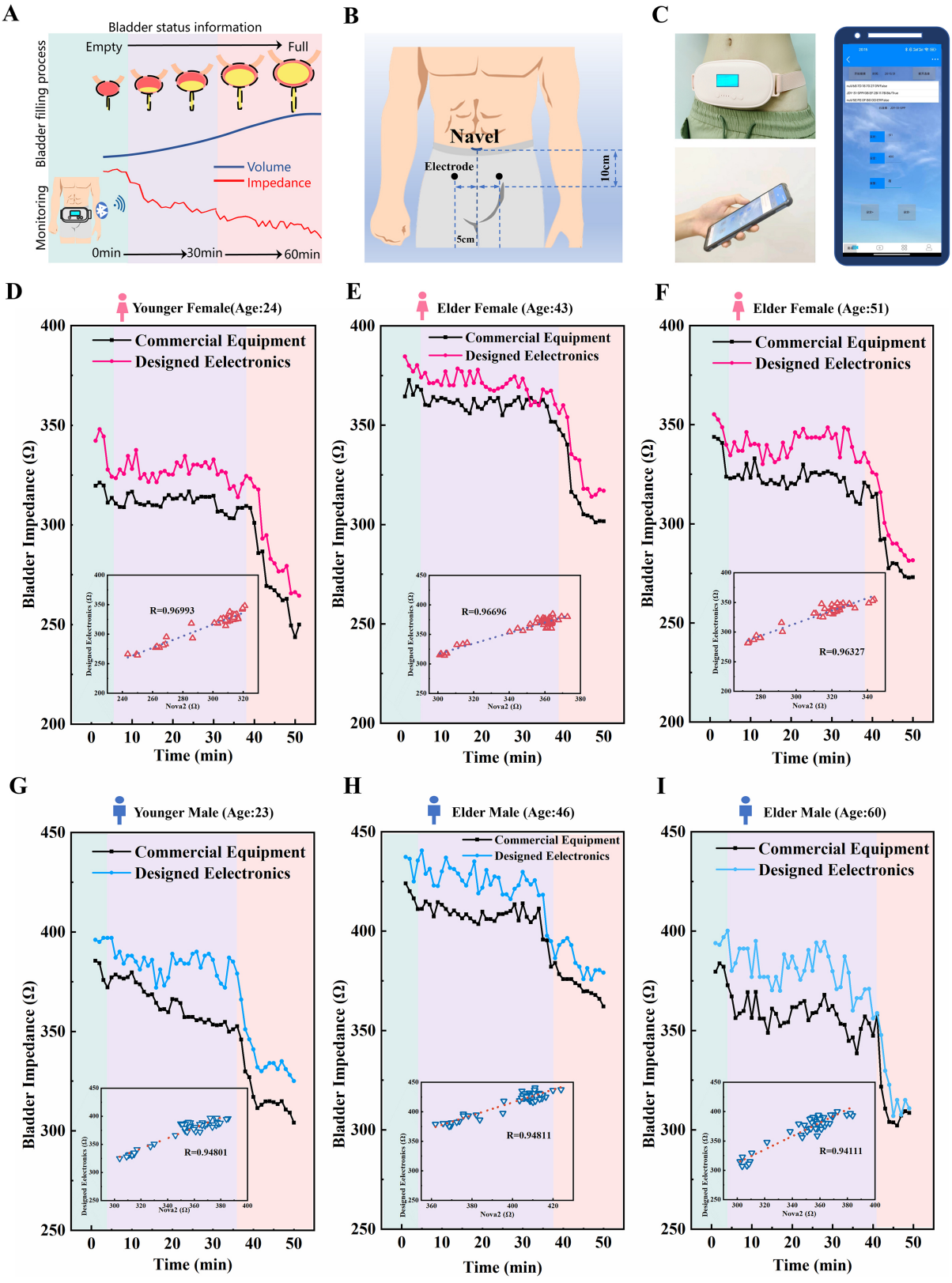

Figure 4. Performance evaluation of biocompatible integrated electronics for non-invasive human bladder volume monitoring in human subjects. (A) Volume and impedance state changes during the passage of time from emptying to filling of the human bladder; (B) Patch electrode mounting locations; (C) Optical images of participants wearing wireless wearable sensors during a bladder test. The data collected were sent to a smartphone and displayed in a developed mobile application; (D-I) The designed electronic device and commercial equipment were employed to monitor the bladder impedance change, and the correlation between the measurement levels of the two devices.

Once the measurements and recordings were complete, the data were subjected to analysis. The mean bladder impedance data obtained from the integrated bladder electronics are presented in Table 1, accompanied by the mean absolute error (MAE), root mean square error (RMSE), and correlation coefficients between the integrated bladder electronics and the commercial equipment. A comparative analysis of Table 1 and Figure 4D-I reveals that the integrated bladder electronics for wireless real-time monitoring exhibit a minor design error and can achieve a strong correlation coefficient of 0.96993 in comparison to the measured data of the commercial equipment. This outcome fulfills the requisite measurement criteria and serves to substantiate the validity and feasibility of the system. The device effectively assesses the user's bladder capacity by collecting signals of changes in bladder impedance, and the low development cost of the device renders it suitable for general application.

CONCLUSIONS

This paper outlines the development of wireless real-time monitoring electronics for human bladder capacity, employing biocompatible material synthesis, BIA and multi-module system integration techniques, aimed at measuring and evaluating bladder impedance and volume changes. The efficacy of this measurement system in quantifying alterations in human bladder impedance has been experimentally verified. Consequently, it is capable of accurately reflecting changes in bladder capacity. Compared with the technical equipment currently in clinical, such as uroflowmetry and US, the device is non-invasive, low-cost, portable and low-power and provides continuous, real-time bladder filling information, thus keeping patients informed of their needs and enhancing their control over bladder voiding function. By predicting the time of urination, it helps patients or their families to prepare in advance and reduce psychological stress, thus improving the quality of life. However, the implementation of the device in clinical and home settings faces several challenges that might be addressed. Firstly, hardware miniaturization, while maintaining performance, remains a significant hurdle, as reducing device size without compromising functionality or power efficiency is crucial, especially in home settings. To realize a more compact design, we aim to optimize the circuit board layout and select smaller components to reduce space requirements and overall device dimensions. Additionally, we will employ flexible printed circuit board (FPCB) technology, leveraging its flexibility to conserve space and better conform to irregular surfaces and curved positions. On the software side, the UI needs to be simplified without sacrificing advanced features, ensuring accessibility for both patients with varying technical expertise and healthcare professionals. Developing intuitive, adaptive UIs, possibly incorporating voice or gesture controls, could enhance usability, particularly for users with physical or cognitive impairments. Looking ahead, further research into advanced microfabrication, energy-efficient algorithms, and AI-driven ubiquitous personalization will be essential to improve device performance, user engagement, and long-term adherence in both clinical and home environments. In conclusion, monitoring changes in bladder impedance over time can be employed to track the progression of bladder-related diseases and treatment effects, facilitate impedance studies of other important units or organs and tissues in the human body, and contribute to the advancement of personalized medicine in the future.

Table 1. The MAE, RMES, and correlation coefficient of the measured values between the designed electronics device and the commercial equipment

Group	Age	MAE/Ω	RMES/Ω	Correlation coefficient
Female 1	24	16.3841	17.1686	0.9699
Female 2	43	11.2448	12.3877	0.9670
Female 3	51	15.6749	16.6148	0.9632
Male 1	23	19.1000	21.2975	0.9480
Male 2	46	15.6127	16.8939	0.9481
Male 3	60	19.3245	21.5747	0.9411

MAE: Mean absolute error; RMES: root mean square error.

DECLARATIONS

Authors' contributions

Made substantial contributions to conception and design of the study and performed data analysis and interpretation: Duan L

Performed data acquisition and provided administrative, technical, and material support: Jin ML

Availability of data and materials

All the data and materials used in our study are available from the corresponding author upon reasonable request.

Financial support and sponsorship

This work was supported by the Young Taishan Scholars Program of Shandong Province (grand no. 201909099), the National Natural Science Foundation of China (grand no. 52003134), the Systems Science Plus Joint Research Program of Qingdao University (grand no. XT2024102) and the Medicine Plus Joint Research Program of Qingdao University (grand no. RZ2400004155) to Jin ML.

Conflicts of interest

All authors declared that there are no conflicts of interest.

Ethical approval and consent to participate

All experiments are conducted in accordance with the declaration of Helsinki and approved by the Ethics Committee Medical College of Qingdao University (QDU-HEC-2024463). All participants were informed about the experimental procedure and research purposes, and have signed the relevant consent forms prior to participation.

Consent for publication

Not applicable.

REFERENCES

1. Semproni, F.; Iacovacci, V.; Menciassi, A. Bladder monitoring systems: state of the art and future perspectives. *IEEE. Access.* **2022**, *10*, 125626-51. DOI
2. Lemack, G. E. Defining the role of overactive bladder treatments in men with lower urinary tract symptoms. *Nat. Clin. Pract. Urol.* **2007**, *4*, 174-5. DOI PubMed
3. Jang, T. M.; Lee, J. H.; Zhou, H.; et al. Expandable and implantable bioelectronic complex for analyzing and regulating real-time

activity of the urinary bladder. *Sci. Adv.* **2020**, *6*, eabc9675. DOI PubMed PMC
4. Klein, R. D.; Hultgren, S. J. Urinary tract infections: microbial pathogenesis, host-pathogen interactions and new treatment strategies. *Nat. Rev. Microbiol.* **2020**, *18*, 211-26. DOI PubMed PMC
5. Kanai, A. J. Afferent mechanism in the urinary tract. *Handb. Exp. Pharmacol.* **2011**, *202*, 171-205. DOI PubMed
6. Sands, J. M.; Layton, H. E. Advances in understanding the urine-concentrating mechanism. *Annu. Rev. Physiol.* **2014**, *76*, 387-409. DOI PubMed
7. Griffiths, D. Neural control of micturition in humans: a working model. *Nat. Rev. Urol.* **2015**, *12*, 695-705. DOI PubMed
8. Franken, J.; De, B. H.; Rietjens, R.; et al. X-ray videocystometry for high-speed monitoring of urinary tract function in mice. *Sci. Adv.* **2021**, *7*, eabi6821. DOI PubMed PMC
9. Osman, N. I.; Esperto, F.; Chapple, C. R. Detrusor underactivity and the underactive bladder: a systematic review of preclinical and clinical studies. *Eur. Urol.* **2018**, *74*, 633-43. DOI PubMed
10. Mariano L, Ingersoll MA. The immune response to infection in the bladder. *Nat. Rev. Urol.* **2020**, *17*, 439-58. DOI PubMed
11. Kwon, J.; Kim, D. Y.; Cho, K. J.; et al. Pathophysiology of overactive bladder and pharmacologic treatments including β3-adrenoceptor agonists -basic research perspectives. *Int. Neurourol. J.* **2024**, *28*, 12-33. DOI PubMed PMC
12. Jonas, C.; Lockl, J.; Röglinger, M.; Weidlich, R. Designing a wearable IoT-based bladder level monitoring system for neurogenic bladder patients. *Eur. J. Inf. Syst.* **2024**, *33*, 993-1015. DOI
13. Vasquez, E. J.; Kendall, A.; Musulin, S.; Vaden, S. L. Three-dimensional bladder ultrasound to measure daily urinary bladder volume in hospitalized dogs. *J. Vet. Intern. Med.* **2021**, *35*, 2256-62. DOI PubMed PMC
14. Kothapalli, S. R.; Sonn, G. A.; Choe, J. W.; et al. Simultaneous transrectal ultrasound and photoacoustic human prostate imaging. *Sci. Transl. Med.* **2019**, *11*, eaav2169. DOI PubMed
15. Angermund, A.; Inglese, G.; Goldstine, J.; Iserloh, L.; Libutzki, B. The burden of illness in initiating intermittent catheterization: an analysis of German health care claims data. *BMC. Urol.* **2021**, *21*, 57. DOI PubMed PMC
16. Hadfield-Law, L. Male catheterization. *Accid. Emerg. Nurs.* **2001**, *9*, 257-63. DOI PubMed
17. Zamli, A. H.; Ratnalingam, K.; Yusmido, Y. A.; Ong, K. G. Diagnostic accuracy of single channel cystometry for neurogenic bladder diagnosis following spinal cord injury: a pilot study. *Spinal. Cord. Ser. Cases.* **2017**, *3*, 16044. DOI PubMed PMC
18. Akcay, A.; Yagci, A. B.; Celen, S.; Ozlulerden, Y.; Turk, N. S.; Ufuk, F. VI-RADS score and tumor contact length in MRI: a potential method for the detection of muscle invasion in bladder cancer. *Clin. Imaging.* **2021**, *77*, 25-36. DOI PubMed
19. Cornelissen, S. W. E.; Veenboer, P. W.; Wessels, F. J.; Meijer, R. P. Diagnostic accuracy of multiparametric MRI for local staging of bladder cancer: a systematic review and meta-analysis. *Urology* **2020**, *145*, 22-9. DOI PubMed
20. Morcos, S. K. Computed tomography urography technique, indications and limitations. *Curr. Opin. Urol.* **2007**, *17*, 56-64. DOI PubMed
21. Yu, H.; Liu, Y.; Zhou, G.; Peng, M. Multilayer perceptron algorithm-assisted flexible piezoresistive PDMS/chitosan/cMWCNT sponge pressure sensor for sedentary healthcare monitoring. *ACS. Sens.* **2023**, *8*, 4391-401. DOI PubMed
22. Kumar, M. N.; Muzzarelli, R. A.; Muzzarelli, C.; Sashiwa, H.; Domb, A. J. Chitosan chemistry and pharmaceutical perspectives. *Chem. Rev.* **2004**, *104*, 6017-84. DOI PubMed
23. Ke, C. L.; Deng, F. S.; Chuang, C. Y.; Lin, C. H. Antimicrobial actions and applications of chitosan. *Polymers* **2021**, *13*, 904. DOI PubMed PMC
24. Ben, Z. Y.; Samsudin, H.; Yhaya, M. F. Glycerol: its properties, polymer synthesis, and applications in starch based films. *Eur. Polym. J.* **2022**, *175*, 111377. DOI
25. Paudel, S.; Regmi, S.; Janaswamy, S. Effect of glycerol and sorbitol on cellulose-based biodegradable films. *Food. Packag. Shelf. Life.* **2023**, *37*, 101090. DOI
26. Zeng, H.; Guo, J.; Zhang, Y.; et al. Green glycerol tailored composite membranes with boosted nanofiltration performance. *J. Membr. Sci.* **2022**, *663*, 121064. DOI
27. Kim, J.; Jeerapan, I.; Imani, S.; et al. Noninvasive alcohol monitoring using a wearable tattoo-based iontophoretic-biosensing system. *ACS. Sens.* **2016**, *1*, 1011-9. DOI
28. Liao, W. C.; Jaw, F. S. Noninvasive electrical impedance analysis to measure human urinary bladder volume. *J. Obstet. Gynaecol. Res.* **2011**, *37*, 1071-5. DOI PubMed
29. Simić, M.; Freeborn, T. J.; Šekara, T. B.; Stavrakis, A. K.; Jeoti, V.; Stojanović, G. M. A novel method for in-situ extracting bio-impedance model parameters optimized for embedded hardware. *Sci. Rep.* **2023**, *13*, 5070. DOI PubMed PMC
30. Hafid, A.; Difallah, S.; Alves, C.; et al. State of the art of non-invasive technologies for bladder monitoring: a scoping review. *Sensors* **2023**, *23*, 2758. DOI PubMed PMC
31. Lim, C.; Hong, Y. J.; Jung, J.; et al. Tissue-like skin-device interface for wearable bioelectronics by using ultrasoft, mass-permeable, and low-impedance hydrogels. *Sci. Adv.* **2021**, *7*, eabd3716. DOI PubMed PMC
32. Cheng, T.; Zhang, Y.; Lai, W. Y.; Huang, W. Stretchable thin-film electrodes for flexible electronics with high deformability and stretchability. *Adv. Mater.* **2015**, *27*, 3349-76. DOI PubMed
33. Zhang, J.; Hu, Y.; Zhang, L.; Zhou, J.; Lu, A. Transparent, ultra-stretching, tough, adhesive carboxyethyl chitin/polyacrylamide hydrogel toward high-performance soft electronics. *Nanomicro. Lett.* **2022**, *15*, 8. DOI PubMed PMC
34. Peng, X.; Dong, K.; Zhang, Y.; et al. Sweat-permeable, biodegradable, transparent and self-powered chitosan-based electronic skin with ultrathin elastic gold nanofibers. *Adv. Funct. Mater.* **2022**, *32*, 2112241. DOI

35. Rinaudo, M. Chitin and chitosan: properties and applications. *Prog. Polym. Sci.* **2006**, *31*, 603-32. DOI
36. Ma, Y.; Xin, L.; Tan, H.; et al. Chitosan membrane dressings toughened by glycerol to load antibacterial drugs for wound healing. *Mater. Sci. Eng. C. Mater. Biol. Appl.* **2017**, *81*, 522-31. DOI PubMed
37. Zahed, M. A.; Kim, D. K.; Jeong, S. H.; et al. Microfluidic-integrated multimodal wearable hybrid patch for wireless and continuous physiological monitoring. *ACS. Sens.* **2023**, *8*, 2960-74. DOI PubMed
38. El-hafian, E. A.; Elgannoudi, E. S.; Mainal, A.; Yahaya, A. H. B. Characterization of chitosan in acetic acid: rheological and thermal studies. *Turk. J. Chem.* **2010**, *34*, 47. DOI
39. Giraldo, J. D.; Rivas, B. L. Direct ionization and solubility of chitosan in aqueous solutions with acetic acid. *Polym. Bull.* **2021**, *78*, 1465-88. DOI
40. Li, P.; Deng, Y.; Zou, W.; Ma, Z.; Yang, X.; Zhao, Q. Biosafe Cu-MOF loaded chitosan/gelatin-based multifunctional packaging film for monitoring shrimp freshness. *Food. Hydrocoll.* **2025**, *160*, 110721. DOI
41. Zhou, C.; Bai, J.; Zhang, F.; et al. Development of mussel-inspired chitosan-derived edible coating for fruit preservation. *Carbohydr. Polym.* **2023**, *321*, 121293. DOI PubMed
42. Bakhshandeh, F.; Zheng, H.; Barra, N. G.; et al. Wearable aptalyzer integrates microneedle and electrochemical sensing for in vivo monitoring of glucose and lactate in live animals. *Adv. Mater.* **2024**, *36*, e2313743. DOI
43. Verma, K. D.; Sinha, P.; Ghorai, M. K.; Kar, K. K. Mesoporous electrode from human hair and bio-based gel polymer electrolyte for high-performance supercapacitor. *Diam. Relat. Mater.* **2022**, *123*, 108879. DOI
44. Yuan, Z.; Hou, L.; Bariya, M.; et al. A multi-modal sweat sensing patch for cross-verification of sweat rate, total ionic charge, and Na^+ concentration. *Lab. Chip.* **2019**, *19*, 3179-89. DOI PubMed
45. Hofmann, T.; Helbig, T.; Schindler, F.; et al. Reciprocal skin effect and its realization in a topolectrical circuit. *Phys. Rev. Research.* **2020**, *2*, 023265. DOI
46. Stankiewicz, J. M. Analysis of the influence of the skin effect on the efficiency and power of the receiver in the periodic WPT system. *Energies* **2023**, *16*, 2009. DOI
47. Humphrey, J. Review paper: continuum biomechanics of soft biological tissues. *Proc. R. Soc. Lond. A.* **2003**, *459*, 3-46. DOI
48. Kemp, N. T. A tutorial on electrochemical impedance spectroscopy and nanogap electrodes for biosensing applications. *IEEE. Sensors. J.* **2021**, *21*, 22232-45. DOI
49. Yang, Y.; Wang, J.; Wang, L.; et al. Magnetic soft robotic bladder for assisted urination. *Sci. Adv.* **2022**, *8*, eabq1456. DOI PubMed PMC
50. Gouin, K. H.; Ing, N.; Plummer, J. T.; et al. An N-cadherin 2 expressing epithelial cell subpopulation predicts response to surgery, chemotherapy and immunotherapy in bladder cancer. *Nat. Commun.* **2021**, *12*, 4906. DOI PubMed PMC
51. Swaminathan, N.; Priyanka, P.; Rathore, A. S.; Sivaprakasam, S.; Subbiah, S. Cole-Cole modeling of real-time capacitance data for estimation of cell physiological properties in recombinant Escherichia coli cultivation. *Biotechnol. Bioeng.* **2022**, *119*, 922-35. DOI PubMed
52. Alam, A. U.; Clyne, D.; Jin, H.; Hu, N. X.; Deen, M. J. Fully integrated, simple, and low-cost electrochemical sensor array for in situ water quality monitoring. *ACS. Sens.* **2020**, *5*, 412-22. DOI PubMed
53. Wang, J.; Ke, T.; Hou, M.; Hu, G. The design of home fire monitoring system based on NB-IoT. *IJACSA.* **2022**, *13*, 35-42. DOI
54. Vázquez-López, A.; Del, R. S. J. S.; de, V. J.; Ao, X.; Wang, D. Y. All-fabric triboelectric nanogenerator (AF-TENG) smart face mask: remote long-rate breathing monitoring and apnea alarm. *ACS. Sens.* **2023**, *8*, 1684-92. DOI PubMed
55. Mahapatra, S.; Kumari, R.; Chandra, P. Printed circuit boards: system automation and alternative matrix for biosensing. *Trends. Biotechnol.* **2024**, *42*, 591-611. DOI PubMed
56. Fonseca, L. A. L. O.; Iano, Y.; Oliveira, G. G. D.; et al. Automatic printed circuit board inspection: a comprehensible survey. *Discov. Artif. Intell.* **2024**, *4*, 81. DOI
57. Ha, H.; Qaiser, N.; Yun, T. G.; Cheong, J. Y.; Lim, S.; Hwang, B. Sensing mechanism and application of mechanical strain sensor: a mini-review. *FU. Mech. Eng.* **2023**, *21*, 751. DOI
58. Gaubert, V.; Gidik, H.; Koncar, V. Smart underwear, incorporating textrodes, to estimate the bladder volume: proof of concept on a test bench. *Smart. Mater. Struct.* **2020**, *29*, 085028. DOI
59. Li, Y.; Peng, Y.; Yang, X.; et al. Analysis of measurement electrode location in bladder urine monitoring using electrical impedance. *Biomed. Eng. Online.* **2019**, *18*, 34. DOI PubMed PMC
60. Freeborn, T. J.; Elwakil, A. S.; Maundy, B. Compact wide frequency range fractional-order models of human body impedance against contact currents. *Math. Probl. Eng.* **2016**, *2016*, 1-10. DOI